RSC Advances

ROYAL SOCIETY OF CHEMISTRY

www.rsc.org/advances

Journal Name

RSCPublishing

ARTICLE

Sweet Potato-derived Carbon Nanoparticles as Anode for Lithium Ion Battery

Cite this: DOI: 10.1039/x0xx00000x

Received ooth January 2012,
Accepted ooth January 2012

DOI: 10.1039/x0xx00000x

www.rsc.org/

Peng Zheng,[*a] Ting Liu,[a] Jinzheng Zhang,[a] Lifeng Zhang,[a] Yi Liu,[a] Jianfeng Huang,[a] and Shouwu Guo,[*a, b]

Consumption of lithium ion batteries (LIBs) has been exploded in recent years, which on the other hand demands abundant and low-cost electrode materials. Sweet potato is a worldwide dicotyledonous plant and has usually a high yield. In the work, using the sweet potato as raw materials, carbon nanoparticles were prepared through a hydrothermal carbonization approach followed by a high temperature annealing. We demonstrate that with the as-prepared carbon nanoparticles as anode, the lithium ion battery shows the first discharge capacity as high as 965 mAh g^{-1} at a current rate of 100 mA g^{-1}. Considering the bio-renewable advantage and facile fabrication procedure, the carbon nanoparticle derived from the sweet potatoes should be sustainably satisfying the increasing consumption of the anode materials for LIBs.

Introduction

Lithium ion batteries (LIBs) have been developed as one of the main power storage devices for portable electronic devices, electric/hybrid vehicles, and most probably as stationary electricity storage setup.[1,2] It was reported that the LIBs production might be tremendously increased from 630 billion of units in 2010 to 3500 billion in 2015.[3] In the most commercialized LIBs, graphite is commonly used as anode owing to its low cost and low electrochemical potential in respect to lithium metal.[4-6] However, the specific capacity and rate capability of graphite and graphitized carbon materials still limit their practical applications in the power LIBs used in electric/hybrid vehicles. Recent years, intensive efforts have been directed to various novel carbonaceous materials such as carbon nanotubes[7-9], nanofibers[10-12], and graphene[13,14] to exploit their potential applications as anode materials. It was illustrated that most of aforementioned materials assumed high reversible capacity and good rate performance, but their bulk scale productions are still challenging. Alternatively, the carbon materials converted from biomasses, such as human hair[15], pomelo peels[16], peat moss[17], wheat straw[18], rice husk[19,20], alginic acid[21], mangrove charcoal[22], cherry stones[23], and coffee shells[24] have also been extensively investigated due to their abundance, low cost, easy processing and bio-renewability. It has been illustrated that most of the biomass-derived carbon materials exhibit good electrochemical performances as anodes for LIBs. For example, the banana peel pseudographite as the anode for LIBs offers a specific capacity of 1090 mAh g^{-1} at 50 mA g^{-1} [25]. The wheat straw derived porous carbon as anode possesses an ultrahigh rate capability of 344 mAh g^{-1} at 18.5 A g^{-1} [18]. The rice husk-derived carbon anode shows a specific capacity of 403 mAh g^{-1} after 100 cycles at 75 mA g^{-1} [19]. The carbonized carbohydrates and sugar have also been investigated as the anode for LIBs[26,27]. For instance, Huang and co-workers synthesized hard carbon sphere with uniform nanopores from carbonization sugar and the 10th cycle's capacity is about 430 mAh g^{-1}.[28] Chen *et al.* prepared spherical hard carbon-derived from potato starch and used as the anode of LIBs.[29] Shu and co-workers reported nanosized hard carbon spheres generated from glucose and demonstrated that reversible lithium ion storage capacity of the as-prepared carbon spheres can reach to 525 mA h g^{-1}.[26]

Sweet potato is a worldwide grown dicotyledonous plant with usually high yield. For instance, in 2011, the average yield over the word was about 106.5 tons per hectare.[30] The main components of sweet potato are carbohydrates (20.1%), starch (12.7 %), sugar (4.18 %), dietary fibre (3 %), and water (~

50%).[31] In principle, the sweet potatoes should be carbonized easily and the as-derived carbon materials would be found appropriate for the anode of LIBs. Herein, we firstly describe the carbonization of sweet potato either through a direct pyrolysis process or through a hydrothermal carbonization followed by pyrolysis treatment, from which carbon bulk materials and carbon nanoparticles were obtained, respectively. The electrochemical performances of the LIBs using the as-prepared carbon materials as anodes were studied. It was illustrated that the specific lithium ion storage capacity of carbon nanoparticles produced through a hydrothermal carbonization followed by pyrolysis treatment is about 1.8 times higher than that of the bulk carbon materials through a direct pyrolysis process.

Experimental Section

Carbonization of sweet potato

The raw sweet potatoes were cultivated in Changan County (Shaanxi，P. R. China). Before the carbonizations, the sweet potato was peeled, cleaned using deionized water thoroughly, dried at room temperature, and finally cut into thin slices (Fig.S1b). For direct pyrolysis carbonization, in a typical experiment, 10 g of sweet potatoes slices were loaded in a tubular furnace and heated at 800 ^{o}C for 2 h in Ar atmosphere. The as-obtained product was denoted as DPC particles. To carbonize the sweet potato through the hydrothermal followed by pyrolysis, 3 g of sweet potatoes slices and 35 ml deionized water were placed in a 50 ml Teflon-lined autoclave and heated at 160 ^{o}C for 10 h first. After being cooled to room temperature naturally, the solid product was collected and washed with deionized water for 3 times, and was named as HTC particles. Then, the HTC particles was annealed further at 800 ^{o}C (heating rate, 5 ^{o}C min^{-1}) for 2 h under Ar atmosphere in a tubular furnace, and the final product was denoted as HTPC particles.

Characterization

X-ray powder diffraction (XRD) patterns were acquired on a Rigaku D/MAX2200PC diffractometer operated at room temperature with Cu Kα (λ =1.54178 Å) radiation. Raman spectra were recorded at room temperature on an InVia confocal Raman microscope system equipped with a 532 nm laser excitation. The specific surface area and porous characteristics were determined with an automated gas adsorption apparatus (Micromeritics, ASAP 2020) using liquid nitrogen adsorption at 77 K. Chemical composition analyses were performed on X-ray photoelectron spectroscopy (XPS) system (ULVAC-PHI5000) using monochromatic Al Kα X-ray source. The morphologies of as-prepared carbon materials were observed by transmission electron microscopy (TEM) (FEI Tecnai F20 microscope) and scanning electron microscopy (SEM) (Rigaku S4800). For observing the morphology of pristine sweet potato, the slices were dried at 80 °C for 10 h under vacuum, and then grinded in to power.

Electrode fabrication and electrochemical measurements

The electrochemical property measurements were conducted on 2032 coin cells using the as-prepared carbon materials as anodes (the working electrode). The working electrode was prepared by mixing the as-obtained carbon materials, conducting agent (Super P), and polyvinylidene fluoride (PVDF) (in N-methyl-2-pyrrolidone) with a weight ratio of 80 : 10 : 10. The obtained slurry was coated onto a copper foil and dried at 120 ^{o}C for 10 h under vacuum. The foil was finally cut into circle discs with diameter of 16 mm, which was used as the anode in the 2032 coin cells. Besides, the pure Li foil was utilized as a counter electrode, Celgard 2500 membrane as separator, and 1.0 mol L^{-1} $LiPF_6$ in mixture EC and DMC (1 : 1 in volume) as electrolyte. All the coin cells were assembled in argon-filled glove box. The charge–discharge tests were performed on a Newaresles battery test system (BTS) (Shenzhen, China) in a voltage range of 0.01–3.0 V at different current rates. The capacity was calculated based on the mass of active material. Cyclic voltammetry (CV) was carried out at room temperature on an electrochemical workstation (CHI 660E). Electrochemical impedance spectral measurements were carried out in the frequency range from 100 kHz to 0.01Hz on a CHI 660E electrochemical workstation.

Results and Discussion

The morphologies of carbon materials generated from sweet potato through different processes are shown in Figure 1. The dried pristine sweet potato powders (after the thin sweet potato slices were dried at 80 °C for 10 h under vacuum, and then grinded) have sizes from 5 μm to 20 μm and exhibit irregular morphologies including spheres, ellipsoids, and others (Fig. 1a and Fig.S1) As expected, the XPS spectrum showed that besides trace amount nitrogen the main component of the dried pristine sweet potato powders is of carbon and oxygen (Fig. S2), which is in agreement with the results reported by others[31]. After pyrolysis at 800 ^{o}C for 2 h under Ar atmosphere, the as-obtained products, called DPC particles, assume bulk morphology with the size over 5 μm (Fig. 1b). After a hydrothermal treatment (160 ^{o}C for 10 h), the as-obtained HTC particles become small with the sizes form 2 μm to 4 μm, and accompanied with certain nanosized side products (Fig. 1c). Figure 1d-f show the HTC particles that were further pyrolyzed at 800 ^{o}C for 2 h under Ar atmosphere. The average size of as-obtained nanoparticles (named as HTPC nanoparticles) is of 120 nm. In contrast, even undergoing a similar pyrolysis treatment, the size and morphology of DPC particles is completely different from those of HTPC nanoparticles. This implies that the pre-hydrothermal treatment seems playing a key role in the formation of carbon nanoparticles with sweet potatoes as raw materials.

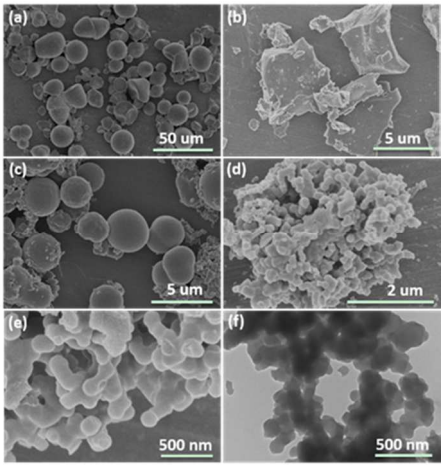

Figure 1. SEM images of (a) pristine sweet potato powder, (b) DPC, (c) HTC, (d) and (e) HTPC particles. (f) TEM image of HTPC particles.

As proposed by Franklin[32], the biomass-derived carbon is usually the hard carbon which may not be graphitized even at relatively high annealing temperature. To evaluate the crystallinity of the as-obtained carbonaceous materials, their X-ray diffraction (XRD) patterns are acquired and shown in Fig. 2a. Obviously, a broad and weak diffraction peak around 2θ = 43° was observed for all DPC and HTPC particles， which can be assigned to the (101) crystallographic planes of graphite, but not for HTC, implying that the as-obtained DPC and HTPC carbon nanoparticles were partially graphitized, which may contribute to their electrical conductivity[19]. The diffraction peak at 2θ = 24° is most prabably originated from the scotch tape used for mounting the powders during the XRD measurement. Figure 2b shows the Raman spectra of the DPC, HTC and HTPC particles, clearly two peaks were observed at 1350 cm^{-1} (D band), and 1590 cm^{-1} (G band) for DPC and HTPC particles, but not for HTC particle. This further shows that the amorphous structural property of HTC, which is in fully agreement with that of the XRD results.

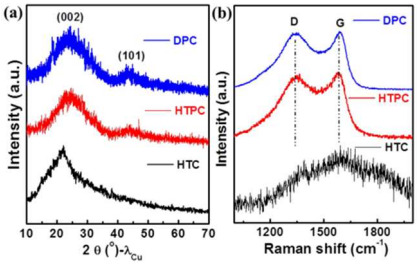

Figure 2. (a) XRD patterns of DPC, HTC and HTPC particles. (b) Raman spectrums of DPC, HTC and HTPC particles.

To further elucidate the chemical compositions of the HTC, HTPC and DPC particles and their formation mechanism, energy-dispersive X-ray (EDX) and X-ray photoelectron spectroscopy (XPS) measurements were employed, and the results were depicted in Table 1 and Figs. S3 and S4. It could be seen that the main compositions of the as-prepared particles are of C and O, and only traced amount of N was observed in HTC and HTPC, but not in DPC. The N content of HTC is slightly higher than that of HTPC. And the O content is decreased by the order of HTC, DPC and HTPC, which indicates that the content of oxygen groups degree is increased by the sequence of HTPC, DPC and HPC. Figure S4 shows high-resolution C1s and N1s XPS spectra and their fitting curves. The content of C=C configuration of HTC (22.9%) (Fig. S4a) is more than that of HTPC (6.7%) (Fig.S4c). While the amount of DPC (32.9%) (Fig.S4e) has the reverse result. Hence, the cross-linking course is different depending on the carbonization approach and precursor. The variation of pyrolic N and pyridinic N (Fig. S4b, 4d and 4f) could also verify this.

During the mild hydrothermal treament, the sweet potatos were converted into carbon sphere through: dehydration (dehydration of the carbohydrate to form furfural); condensation (polymerization towards polyfurans); carbonization (carbonization via further intermolecular dehydration), which were recognized during the carbon nanosphere preparation with starch or sugar as raw materials.[33] From the coarse surface of sphere (Fig. S5) contrast with the starch sphere[34] and the sugar sphere[35], we deduce that other carbohydrates of sweet potato constitution maybe hydrothermal carbonized and cross-linked with the sphere. The N signal from EDS and XPS could also confirm this, as starch and suagr do not contain nitrogen element. Further pyrolysis process could provide high degree of carbonization. During this process, combining with the variation of the contents and the C=C bonding, we conjecture that some relatively low cross-linking substance decomposes into gaseous products and the heavy cross-linking substance was left, and the reduced yield from HTC to HTPC could also confirm this (Table S1). As most of the low cross-linking substance was decomposed, the size of the particle became small and the nano-particle of HPTC was formed.

Table 1: Chemical composition of HTC, HTPC and DPC materials determined by energy-dispersive X-ray spectroscopy (EDX) and X-ray photoelectron spectroscopy (XPS) measurement.

	EDX (wt %)			XPS (atom %)		
	C	N	O	C	N	O
HTC	72.05	5.39	22.56	70.18	3.36	26.46
HTPC	80.43	4.92	14.65	90.56	2.39	5.81
DPC	78.55	0.61	20.84	80.26	0.07	19.67

The electrochemical performance of the coin cells with the sweet potato-derived HTPC nanoparticles as working anodes were systematically investigated. Figure 3a shows the typical cyclic voltammetry (CV) curves of the coin cells acquired between 0.01 V and 3 V at a scan rate of 0.1 mV s^{-1}. Notably, two peaks at ~1.2 V and ~0.25 V are observed in the first redox cycle. The peak at ~1.2 V only appears in the first cycle which can be attributed to the irreversible Li^+ adsorption, and the formation of SEI film. The SEI film is associated with electrolyte decomposition and the formation of lithium organic compounds.[36] The small oxidation peak at 0.25 V shown in the charge process can be ascribed to the Li^+ extraction from the graphite layers. The 0.01–0.2 V peak corresponds to the reversible insertion of Li^+. The nitrogen (N_2) adsorption–desorption isotherm is shown in Figure S6a, the specific Brunauer–Emmett–Teller (BET) surface area of the HTPC nanoparticles is of 79.1 m^2 g^{-1}. The corresponding pore sizes distributions (PSDs) are calculated usin g a density function theory (DFT) model and are shown in Figure S6b. It can be found that the HTPC nanoparticles contain mainly microspores, but little of mesopores. These microspores may be resulted from the escape of low-molecular gases from carbon matrix during carbonization. The microspores are considered as charge accommodation for carbon-based anode.[18]

Figure 3b shows the 1st, 2nd and 200th charge/discharge profiles of the coin cell with HTPC nanoparticles as working electrode at a current density of 100 mA g^{-1} (about 0.27 C, 1 C equals to 372 mA g^{-1}). The initial discharge/charge capacities are 965 mAh g^{-1}, the low Coulombic efficiency might be resulted from the decomposition of electrolyte and SEI formation on the electrode surface, which is agreement with the result of 1st cycle CV curve, and also the residual oxygen-containing groups in the HTPC particles (see Table 1 and Fig. S4). The oxygen-containing groups may react with Li^+ to form lithium oxide. The performances at different charge–discharge rates are shown in Figure 3c. The working electrode of HTPC nanoparticles showed also manifest rate capability. The charge capacity is of 285 mAh g^{-1} at 0.5 C, 235 mAh g^{-1} at 1 C, 126 mAh g^{-1} at 5 C and 84 mAh g^{-1} at 10 C, respectively. Actually, the coin cells also showed good cycling stabilities. For instance, once the current rate was returned to 0.27C after long time discharge/charge cycling at a vary of current rates, the capacity can increase back to 320 mAh g^{-1}, which is close to the initial capacity at the same current rate. The cycling stability and the

Columbic efficiency are further evaluated by charging–discharging of the coin cells at certain current rate. As shown in Figure 3d, at a current rate of 100 mAh g^{-1}, the capacity of coin cells with the HTPC nanoparticle anode at third discharge/charge cycle is of 328 mAh g^{-1}, and it was retained at 320 mAh g^{-1} after 200 cycles with a capacity loss of only 0.25%. The Columbic efficiency approaches to 98 % after several cycles (Fig.3e), presumably due to incomplete stabilization of SEI.

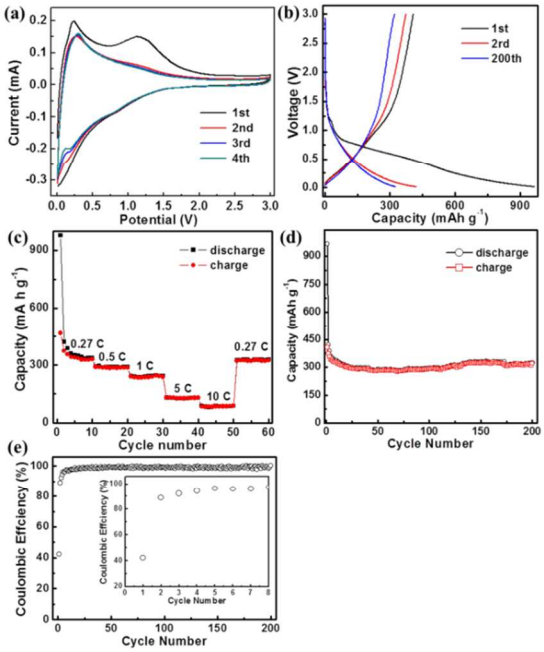

Figure 3. (a) CV curve of the anode of HTPC nanoparticles at a scan rate of 0.1 mV s^{-1} over a potential range of 0.01–3.0 V; (b) Galvanostatic discharge–charge curves of HTPC nanoparticle electrode at a current density of 0.1 A g^{-1}; (c) the rate performances of HTPC as anode from 0.27 C to 10 C; and (d) cycling performance at the current density of 0.1 A g^{-1}; (e) The corresponding columbic efficiency of Fig.3d, the inset is the enlarged image of the first few columbic efficiency.

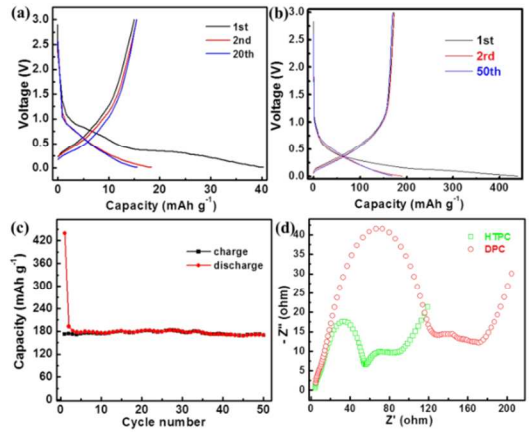

Figure 4. (a) Galvanostatic discharge–charge curves of the coin cells with bulk HTC particles as anode at 0.1 A g^{-1}; (b) The discharge–charge curves of coin cells with DPC particles as anode at 0.1 A g^{-1}; (c) Cycling performance of the coin cell with DPC particles as anode at the current densities of 0.1 A g^{-1}. (d) Typical Nyquist plots the anodes of HTPC and DPC particles.

In contrast, the first cycle discharge capacity of the coin cells with HTC particles as working electrode is only 40 mAh g^{-1}, and decayed to 15.5 mAh g^{-1} after 20 cycles at a current rate of 100 mAh g^{-1} (Fig. 4a), which is much lower than those of the coin cells with the HTPC nanoparticles as anodes. The reason might be that the HTC particles assume bulk morphology and their crystallinity is relatively poorer than that of HTPC nanoparticles.[19] As expected, the DPC particles exhibit much higher capacity than that of HTC particles. The first cycle discharge capacity of the coin cells with the DPC particles as anode can reach to 440 mAh g^{-1} at current rate of 100 mAh g^{-1} and retained at 170 mAh g^{-1} after 50 cycles (Fig.4b, c). But, it is still lower than that of the coin cells with HTPC nanoparticles as anode. This may rise from the size differences between DPC and HTPC nanoparticles. Usually, the small particle has short path way for the Li^+ and electron diffusion. The nanoparticles have also larger specific surface area than that of the bulk, which should be beneficial for the contact between electrode and lithium ion from electrolyte. To further verify the electron transport properties of HTPC and DPC particles, their electrochemical impedance spectroscopy (EIS) data were acquired (Fig. 4d). The impedance at high frequency in the impedance spectra corresponds to the charge transfer resistance (Rct) at the interface of electrode and electrolyte. As can be seen, the diameter of the semicircle for the anode of HTPC nanoparticles has a lower value than that of the DPC particles, indicating a remarkable decrease in charge transfer resistance. And compared with the bulk, the nano-particle has larger specific area, these should be main reason why the coin cells with HTPC nanoparticles as anode assume better electrochemical performances than those with DPC particles as anode.

Conclusions

In summary, carbon nanoparticles were prepared using sweet potatoes as raw materials through a facile hydrothermal procedure followed by short time hydrolysis. Using the as-prepared carbon nanoparticles as anode materials for LIBs, the coin cells show high specific lithium ion storage capacity of 965 mAh g^{-1} at the first discharge cycle, 328 mAh g^{-1} at third discharge cycle, and it was retained at 320 mAh g^{-1} after 200 cycles with a capacity loss of only 0.25% at a current density of 100 mA g^{-1}. It was also demonstrated that the unique nanoparticle morphology, larger specific area, and enriched porous structure within the carbon particles might play key roles in the manifest electrochemical performances as anode for LIBs. Given abundant and renewable resource of sweet potatoes, the as-prepared carbon nanoparticles should satisfy the increasing demand of anode materials for LIBs.

Acknowledgements

The authors acknowledge the financial supports from national "973" Preliminary program (No. 2014CB260411) of China, Fund for Sanqin Scholar (No. BJ11-26), China Postdoctoral Science Foundation funded project (No. 2014M562514XB), and National Natural Science Fund of China (No. 21203116)

Notes and references

[a] School of Materials Science and Engineering, Shaanxi University of Science and Technology, Xian 710021, Shaanxi, P. R. China.

[b] Department of Electronic Engineering, School of Electronic Information and Electrical Engineering, Shanghai Jiao Tong University, Shanghai 200240, P. R. China

Electronic Supplementary Information (ESI) available: See DOI: 10.1039/b000000x/

1 W. Xu, J. Wang, F. Ding, X. Chen, E. Nasybulin, Y. Zhang and J.-G. Zhang, Energy Environ. Sci., 2014, **7**, 513-537.
2 L. Dimesso, C. Forster, W. Jaegermann, J. P. Khanderi, H. Tempel, A. Popp, J. Engstler, J. J. Schneider, A. Sarapulova, D. Mikhailova, L. A. Schmitt, S. Oswald and H. Ehrenberg, Chem. Soc. Rev., 2012, **41**, 5068-5080.
3 P. Verma, P. Maire and P. Novák, Electrochim. Acta., 2010, **55**, 6332-6341.
4 E. Peled, C. Menachem, D. Bar‐Tow and A. Melman, J. Electrochem. Soc., 1996, **143**, L4-L7.
5 Y.-W. Cheng, C.-K. Lin, Y.-C. Chu, A. Abouimrane, Z. Chen, Y. Ren, C.-P. Liu, Y. Tzeng and O. Auciello, Adv. Mater., 2014, **26**, 3724-3729.
6 M. B. J. G. Freitas and E. M. Garcia, J. Power Sources., 2007, **171**, 953-959.
7 Y. Chen, X. Li, K. Park, J. Song, J. Hong, L. Zhou, Y.-W. Mai, H. Huang and J. B. Goodenough, J. Am. Chem. Soc., 2013, **135**, 16280-16283.
8 R. H. Baughman, A. A. Zakhidov and W. A. de Heer, Science, 2002, **297**, 787-792.
9 X. Chen, H. Zhu, Y.-C. Chen, Y. Shang, A. Cao, L. Hu and G. W. Rubloff, ACS Nano, 2012, **6**, 7948-7955.
10 X.-B. Cheng, G.-L. Tian, X.-F. Liu, J.-Q. Nie, M.-Q. Zhao, J.-Q. Huang, W. Zhu, L. Hu, Q. Zhang and F. Wei, Carbon, 2013, **62**, 393-404.
11 L. Qie, W.-M. Chen, Z.-H. Wang, Q.-G. Shao, X. Li, L.-X. Yuan, X.-L. Hu, W.-X. Zhang and Y.-H. Huang, Adv. Mater., 2012, **24**, 2047-2050.
12 S. Xin, Y.-G. Guo and L.-J. Wan, Acc. Chem. Res., 2012, **45**, 1759–1769.
13 Y. Zhao, J. Feng, X. Liu, F. Wang, L. Wang, C. Shi, L. Huang, X. Feng, X. Chen, L. Xu, M. Yan, Q. Zhang, X. Bai, H. Wu and L. Mai, Nat Commun, 2014, 5, doi:10.1038/ncomms5565.
14 J. Zhang, H. Yang, G. Shen, P. Cheng, J. Zhang and S. Guo, Chem. Commun., 2010, **46**, 1112-1114.
15 W. Qian, F. Sun, Y. Xu, L. Qiu, C. Liu, S. Wang and F. Yan, Energy Environ. Sci., 2014, **7**, 379-386.
16 K.-l. Hong, L. Qie, R. Zeng, Z.-q. Yi, W. Zhang, D. Wang, W. Yin, C. Wu, Q.-j. Fan, W.-x. Zhang and Y.-h. Huang, J. Mater. Chem. A., 2014, **2**, 12733-12738.
17 J. Ding, H. Wang, Z. Li, A. Kohandehghan, K. Cui, Z. Xu, B. Zahiri, X. Tan, E. M. Lotfabad, B. C. Olsen and D. Mitlin, ACS Nano, 2013, **7**, 11004-11015.
18 L. Chen, Y. Zhang, C. Lin, W. Yang, Y. Meng, Y. Guo, M. Li and D. Xiao, J. Mater. Chem. A., 2014, **2**, 9684-9690.
19 L. Wang, Z. Schnepp and M. M. Titirici, J. Mater. Chem. A., 2013, **1**, 5269-5273.
20 G. T.-K. Fey and C.-L. Chen, J. Power Sources., 2001, 97–98, 47-51.
21 X.-L. Wu , L.-L. Chen , S. Xin, Y.-X. Yin, Y.-G. Guo, Q.-S. Kong and Y.-Z. Xia, ChemSusChem, 2010, **3**, 703-707.
22 T. Liu, R. Luo, W. Qiao, S.-H. Yoon and I. Mochida, Electrochim. Acta , 2010, **55**, 1696-1700.
23 J. C. Arrebola, A. Caballero, L. Hernán, J. Morales, M. Olivares-Marín and V. Gómez-Serrano, Journal of J. Electrochem. Soc., 2010, **157**, A791-A797.
24 Y. J. Hwang, S. K. Jeong, K. S. Nahm, J. S. Shin and A. Manuel Stephan, J. Phys. Chem. Solids, 2007, **68**, 182-188.
25 E. M. Lotfabad, J. Ding, K. Cui, A. Kohandehghan, W. P. Kalisvaart, M. Hazelton and D. Mitlin, ACS Nano, 2014, **8**, 7115–7129.
26 J. Shu, M. Shui, D. Xu, S. Gao, X. Li, Y. Ren, L. Hou, J. Cui, J. Xu and Z. Zhu, J. Electroanal. Chem., 2011, **657**, 187-191.
27 F. Zhang, C. Liang, X. Wu and H. Li, Angew. Chem., 2014, **53**, 8498-8502.
28 Q. Wang, H. Li, L. Chen and X. Huang, Solid State Ionics, 2002, **152–153**, 43-50.
29 W. Li, M. Chen and C. Wang, Mater Lett., 2011, **65**, 3368-3370.
30 Raymundo R, Asseng S, Cammarano D, Quiroz R. Field Crops Res. 2014, **166**, 173-85.
31 http://en.wikipedia.org/wiki/Sweet_potato#Yields_of_sweet_potato_crop
32 Peter J. F. Harris., Interdiscip. Sci. Rev. 2001, **26**, 204-210.
33 M.-M. Titirici and M. Antonietti, Chem. Soc. Rev., 2010, 39, 103-116.
34 D. Jin, X. Yang, M. Zhang, B. Hong, H. Jin, X. Peng, J. Li, H. Ge, X. Wang, Z. Wang and H. Lou, Mater. Lett., 2015, 139, 262-264.
35 X. Sun and Y. Li, Angew. Chem., 2004, 43, 597-601.
36 W.-Q. Tian, X.-Y. Wu, K.-X. Wang, Y.-M. Jiang, J.-F. Wang and J.-S. Chen, RSC Adv., 2013, **3**, 10823-10827.